JOURNAL OF MECHANICAL ENGINEERING AND SCIENCES
ISSN: 2289-4659 e-ISSN: 2231-8380
VOLUME 18, ISSUE 2, 2024, 10026 – 10045
DOI: https://doi.org/10.15282/jmes.18.2.2024.5.0792

RESEARCH ARTICLE

Numerical study of thermal and hydrodynamic characteristics of turbulent flow in hybrid corrugated channels with different wave profiles

D. Uysal[1], S. Akçay[2]*

[1] Institute of Science and Technology, Faculty of Engineering, Çankırı Karatekin University, 18100 Çankırı, Turkey
[2] Department of Mechanical Engineering, Faculty of Engineering, Çankırı Karatekin University, 18100 Çankırı, Turkey
Phone: +903762189532; Fax: +903762189536

ABSTRACT - The geometry of the wave profiles used in corrugated channels affects the flow and thermal characteristics. It is possible to increase thermal and hydraulic performance by simply changing the groove profile's shape without using any additional energy. Therefore, this numerical study focused on the flow and thermal performance of different groove profiles in hybrid corrugated channels. The study was conducted using the finite volume method (FVM) with the standard k-ε turbulence model. The study consisted of three different hybrid corrugated channel flows created by combining the rectangular groove profile and the circular, trapezoidal, and triangular-shaped groove profiles separately. In addition, the numerical results were compared with the rectangular corrugated duct and the straight duct. The corrugated surfaces were kept constant at T_w = 380 K. Nusselt number, friction factor, and performance factor were calculated for different Reynolds numbers (2000 ≤ Re ≤ 10000). Images of flow and temperature contours were presented to demonstrate the effects of groove profiles. According to the numerical findings, the combination of the rectangular groove profile with other groove profiles significantly improved the heat transfer without any significant increase in pressure drop. The thermal performance was significantly affected by Re and the hybrid groove profiles. The rectangular-circular and rectangular-trapezoidal hybrid corrugated channels showed similar behaviors in terms of hydraulic and thermal attitude. It was determined that heat transfer in rectangular-circular and rectangular-trapezoidal hybrid groove profiles improved 4.38 times compared to straight ducts at Re = 8000 and 1.23 times compared to rectangular corrugated ducts at Re = 2000.

ARTICLE HISTORY
Received : 18th Oct. 2023
Revised : 28th Feb. 2024
Accepted : 22nd Mar. 2024
Published : 28th June 2024

KEYWORDS
Hybrid wave profile
Heat transfer
Performance factor
Pressure drop
Turbulent flow

1. INTRODUCTION

Increasing, intensifying, and improving heat transfer play a critical role in many areas, such as heat exchangers [1, 2], chemical and food processes [3, 4], cooling of electronic devices [5-7], and thermal management of nuclear reactors [8]. Heat transfer improvement methods attract great attention in engineering applications due to the fact that they promote the effective use of limited energy resources, increase the efficiency of energy systems, provide energy savings, and reduce energy costs. These methods are generally classified as active, passive, and combined heat transfer improvement methods [9, 10]. Compared to active methods, passive methods are advantageous because they do not require an external power input to increase thermal efficiency, and they are more reliable and economical since they do not contain mechanical parts [11]. Therefore, the interest in passive techniques is increasing day by day. Passive methods include arrangements made in the channel geometry, extended surfaces, and modifications such as pin/fin, winglet, and turbulator added to the channel [12-14]. Many numerical and experimental research involving these modifications have been carried out, and the results of these studies have indicated that the baffles/winglets/turbulators provide significant enhancement in heat transfer with an increment in pressure drop [11, 15, 16]. In a numerical study, Feng et al. [17] investigated the thermal enhancement and hydraulic performance of a triangular corrugated duct including trapezoidal baffles in different arrangements. Their study results revealed that the friction factor and Nu increased by 3.5 times and 1.7 times, respectively. Although these modifications added into the channel improve heat transfer depending on the geometric and flow parameters used, they cause a significant increase in pressure drop because they create resistance to flow [18]. This will result in more energy consumption, and thereby lead to an increase in heat transfer and pumping costs. Therefore, researchers focused on wavy/corrugated surfaces, which are widely used among passive methods [19, 20]. It has been reported that wavy channels have an effective potential in improving heat transfer of thermal devices since they create additional flow areas that promote heat transfer and improve flow mixing [21]. For this reason, wavy/corrugated channels are widely used in many heating and cooling applications, solar collectors, and especially heat exchangers. Many wave profiles have been investigated to improve hydraulic and thermal performance in these applications [22].

In previous studies, the thermohydraulic behaviors of corrugated/wavy channels with a uniform wave profile have been investigated for different fluids and flow situations. As a result of these studies, it has been declared that wavy/corrugated ducts provide a significant improvement in thermal performance with a slight increase in pressure drop compared to straight ducts [23-25]. The effects of different groove profiles on thermal and hydraulic behavior in channel

*CORRESPONDING AUTHOR | S. Akçay | ✉ selmaakcay@karatekin.edu.tr

flows have also been investigated in many experimental and numerical studies [26-28]. Among these groove profile geometries, sinusoidal wave profile [29, 30], semi-circular groove profile [31-33], triangular groove profile [34-37], trapezoidal groove profile [38, 39] and rectangular groove profile [40], and new type groove profiles [41-43] have been examined for different parameters. Some researchers have examined the impacts of geometric parameters on the groove profile of corrugated channels. In these studies, flow and heat transfer characteristics have been investigated by changing geometric parameters such as the length and amplitude of the wave profile, the distance between the wave profiles, and the arrangement of the profiles (symmetrical, staggered, etc.) [44, 45]. Ajeel et al. [46] analyzed the hydraulic and thermal performance of a turbulent nanofluid case in a wavy channel with trapezoidal groove profiles placed in a symmetrical and staggered arrangement by using a finite volume approach and compared the results with smooth duct flow. It was noticed that the heat transfer performance of the trapezoidal grooved channel in the symmetrical arrangement was higher than that of the straight channel and staggered arrangement. In other studies of Ajeel et al. [47], the authors experimentally and numerically examined the turbulent flow heat transfer of two different channels with inward circular and inward trapezoidal waves in SiO2-water nanofluid flow, and they compared the results with the smooth duct. They found that the pressure drop and Nu in the trapezoidal wavy duct were higher than in the circular duct. The results showed that the maximum enhancement rate was acquired as 3.1 for Re = 10000 in the trapezoidal wavy duct and it was recommended that the trapezoidal profile structure is a good choice for heat exchangers.

Zheng et al. [42] conducted a numerical study on heat transfer in turbulent nanofluid flow of triangular and circular barriers with different heights on the surfaces of a rectangular channel. They reported that the pumping power increased as the height of the barriers increased and explained that the circular barriers provided higher Nusselt number and performance value than the triangular barriers. Choudhary et al. [48] investigated the heat transfer and hydraulic behaviors of corrugated channels in heat exchangers by comparing them with the smooth duct, and they determined that the wavy channel was superior to the corrugated duct in terms of hydraulic, and the thermal performance of the wavy duct increased by 28.46% compared to the straight channel. However, they found that the pressure drop in the corrugated channel was also higher. In a numerical study, Naderifar et al. [49] simulated the impacts of the number of grooves (1-5 grooves) and the length of the fins (5-10 mm) on thermal performance in a rectangular grooved duct with fins on the inner surface in laminar case. It was reported that Nu was higher in the channel with 2 waves compared to the smooth duct, and the best thermal improvement was obtained when the fin height was 7.5 mm. Other researchers have examined the thermal and hydrodynamic behavior of multiple channel flows with different wave profiles and compared thermo-hydraulic performance values. Zhang and Che [50] examined the heat transfer and flow characteristics in different wavy ducts (sinusoidal, rectangular, trapezoidal, elliptical, and triangular-shaped) and revealed that trapezoidal wave profile provided higher heat transfer and friction factor than other channels. Ahmet et al. [51] conducted a numerical study investigating the heat transfer and fluid flow in grooved ducts with different geometries (sinusoidal, trapezoidal, and triangular). They noticed that, compared to other profiles, while the maximum Nusselt number and pressure loss were achieved in the trapezoidal wave, the sinusoidal wave profile provided the highest thermohydraulic performance. The results of Salami et al. [52] indicated that the highest thermal performance was provided in the trapezoidal corrugated duct, while the best thermo-hydraulic performance was provided in the sinusoidal wavy duct. Ameur and Sahel [2] reported that in rectangular, triangular, and semicircular wavy channels, while heat transfer increased, pumping power decreased. Ajeel et al. [53] carried out a computational study to compare the thermal behavior of three different groove profiles in a corrugated channel. They used different particle volume ratios ($0 \leq \varphi \leq 0.08$) and different Reynolds numbers ($10000 \leq Re \leq 30000$) of ZnO-water nanofluid. As a result, they found that the trapezoidal wavy channel provided higher thermal performance than other models. They also reported that within the given Reynolds number range, the highest pressure drop occurred in the circular duct, and it was followed by the trapezoidal and the house-shaped duct, respectively. Shahsavar et al. [54] examined the thermal and hydraulic characteristics of nanofluids in different wavy ducts (sinusoidal, triangular, and trapezoidal), and reported that the sinusoidal corrugated duct provided higher thermal enhancement. In a numerical study, Togun et al. [32] investigated the heat transfer behavior of nanofluids in a circular wavy duct for different modifications of ribs at $10000 \leq Re \leq 25000$. They indicated that the heat transfer increased with Re.

The studies mentioned above show that the geometric shape of the groove profile in corrugated channels affects the hydraulic and thermal performance. Among different wave profiles, rectangular and trapezoidal wave profiles provide higher thermal performance due to their high surface area, while circular and sinusoidal wave profiles require lower pumping power. Considering these advantages and disadvantages of wave profiles, the idea of combining different wave profiles in a single channel design has emerged. Therefore, new channel designs with hybrid waves involving the combination of wave profiles with different geometries have been recently investigated [55]. Ahmad et al. [28] conducted a numerical study to examine the impact of the amplitude of different groove profiles (rectangular, sinus-shaped, and V-shaped) in a mini channel on thermal performance under turbulent nanofluid flow conditions. They found that the highest thermal improvement was 22.19 % in the rectangular wavy mini-channel when the wavelength/amplitude ratio was 0.12. Khan et al. [43] numerically investigated the effects of the geometric parameters of the wavy tube at different Reynolds numbers by using a tube geometry with a new groove model in parabolic trough solar collectors to increase energy efficiency. As a result, they proposed an optimum model for the wavy absorber tube. Kumar et al. [56] conducted a numerical study on the entropy production, heat transfer, and pressure drop at different Reynolds numbers ($15000 \leq Re \leq 37500$) in hybrid wavy channel flows consisting of the combination of three different profiles in the form of arc, trapezoidal, and triangular. They reported that the highest Nu was obtained at Re = 37500 in the inward arc-outward

triangular hybrid wave profile. In inward-outward hybrid corrugations, the lowest friction factor was obtained in the arc-tri profile, while the highest friction factor was found in the trapezoidal-arc profile.

As understood, in the studies conducted so far on the use of wavy channels to increase heat transfer, a uniform wave profile (triangular, trapezoidal, sinusoidal, or circular, etc.) has generally been preferred. In these studies, the effects of many geometric parameters, such as the geometry of the groove profile, distance between groove profiles, wavelength, wave amplitude, and wave angle, were examined. In addition, multiple channels with different groove profiles were compared. However, there are very few studies examining the hydrodynamic and thermal characteristics in a hybrid wavy duct containing a combination of different wave profiles. Therefore, in this study, the hydrodynamic and thermal behavior of turbulent flow in three different hybrid corrugated ducts consisting of the combination of triangular, trapezoidal, and circular wave profiles with a rectangular wave profile was comprehensively simulated. In addition, the numerical study was compared with rectangular groove channel and straight channel flow. The main purpose of this study is to determine the wavy channel structure, which includes different combinations of commonly used groove profiles (triangular, circular, trapezoidal, and rectangular) to increase heat transfer without causing a significant increase in pressure drop, and to guide channel designers in this regard.

2. MATERIALS AND METHODS

2.1 Description of the Physical Model

Figure 1 shows two dimensional geometric schemes of corrugated channels with different groove profiles. The hybrid channel designs include a combination of rectangular wave profile and three different groove profiles (circular, trapezoidal, and triangular-shaped) separately. Maximum and minimum height of the channels are H_2 = 38 mm and H_1 = 18 mm. There is an unheated flat section of L_1 = 360 mm and L_3 = 500 mm at the inlet and outlet of the channels, respectively. The length of the grooved part of the duct is L_2 = 500mm. The maximum width of the wave profile is a = 20 mm, and the distance between the wavy sections is b = 40 mm. The side lengths of the triangular wavy profile are equal. The trapezoidal wave profile is also an equilateral. Heated length of the channel (L_2) includes a total of 9 wave profiles.

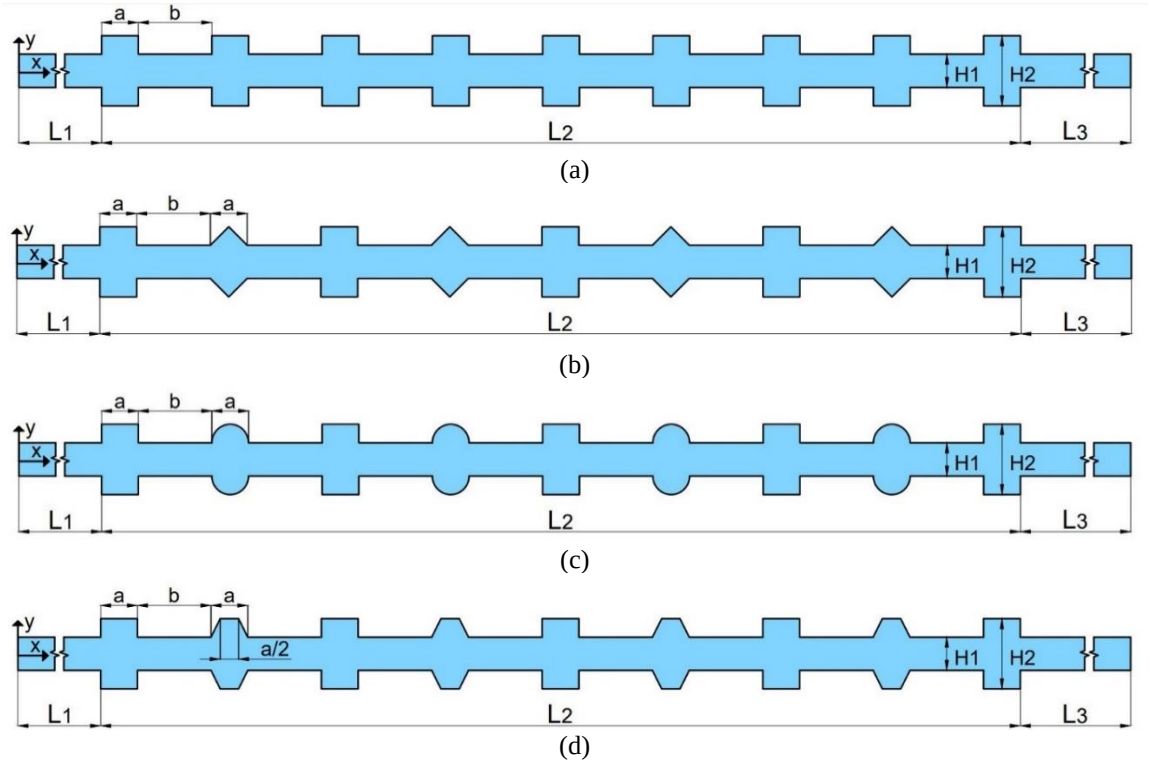

Figure 1. The channel geometries with different wave profiles: (a) rectangular, (b) rectangular-triangular hybrid, (c) rectangular-circular hybrid and (d) rectangular-trapezoidal hybrid

2.2 Governing Equations and Assumptions

The solutions of the numerical study were carried out with the help of ANSYS Fluent program [57]. Water was used as the fluid. Assumptions adopted for the solutions are listed as follows:

- The fluid is Newtonian, single phase and incompressible.
- It is assumed that fluid properties do not change with temperature.
- The flow field is two-dimensional. The flow is fully developed, turbulent and steady.

- Viscous dissipation is neglected.
- There is no internal heat production within the channel.
- The effect of body forces (such as gravity) is not considered.
- It is accepted that heat transfer does not occur by radiation.

Considering the above assumptions, the conservation equations can be presented as in the following equations:

Continuity equation:

$$\frac{\partial}{\partial x_i}(\rho \bar{u}_i) = 0 \tag{1}$$

Momentum equation:

$$\frac{\partial}{\partial t}(\rho \bar{u}_i) + \frac{\partial}{\partial x_j}(\rho \bar{u}_i \bar{u}_j) = -\frac{\partial \bar{p}}{\partial x_i} + \frac{\partial}{\partial x_j}\left[(\mu + \mu_t)\left(\frac{\partial \bar{u}_i}{\partial x_j} + \frac{\partial \bar{u}_j}{\partial x_i}\right)\right] - \rho\overline{u_i' u_j'} \tag{2}$$

Energy equation:

$$\frac{\partial}{\partial t}(\rho c \bar{T}) + \frac{\partial}{\partial x_j}(\rho \bar{u}_i \bar{T}) = \frac{\partial}{\partial x_j}\left[(\Gamma + \Gamma_t)\left(\frac{\partial \bar{T}}{\partial x_j}\right)\right] \tag{3}$$

$$-\rho\overline{u_i' u_j'} = (\mu_t)\left(\frac{\partial u_i}{\partial x_j} + \frac{\partial u_j}{\partial x_i}\right) \tag{4}$$

$$\frac{\partial}{\partial t}(\rho k) + \frac{\partial}{\partial x_i}(\rho k \bar{u}_i) = \frac{\partial}{\partial x_j}\left[\left(\mu + \frac{\mu_t}{\sigma_k}\right)\frac{\partial k}{\partial x_j}\right] + G_k - \rho\varepsilon \tag{5}$$

$$\frac{\partial}{\partial t}(\rho \varepsilon) + \frac{\partial}{\partial x_i}(\rho \varepsilon \bar{u}_i) = \frac{\partial}{\partial x_j}\left[\left(\mu + \frac{\mu_t}{\sigma_\varepsilon}\right)\frac{\partial \varepsilon}{\partial x_j}\right] + C_{1\varepsilon}\frac{\varepsilon}{k}G_k - C_{2\varepsilon}\rho\frac{\varepsilon^2}{k} \tag{6}$$

$$G_k = -\rho\overline{u_i' u_j'}\frac{\partial u_j}{\partial x_i},\ \mu_t = \rho C_\mu \frac{k^2}{\varepsilon},\ \Gamma = \frac{\mu}{Pr},\ \Gamma_t = \frac{\mu_t}{Pr_t} \tag{7}$$

For the constants in the turbulence model, σ_k = 1.0, σ_ε = 1.3, $C_{1\varepsilon}$ = 1.44, $C_{2\varepsilon}$ = 1.92, C_μ = 0.09, and Pr_t = 0.9 were used [40, 58].

2.3 Numerical Solution Method and Boundary Conditions

In the study, the drawings of the wavy channels were created in two dimensions with the Gambit software, and then all channels were divided into cells. The image of the mesh structure created for the rectangular wavy channel is given in detail in Figure 2. To determine the optimal number of elements where the numerical results were not affected by the grid numbers, the mesh independence test was utilized to all the studied wavy channels. As a result of this test, element numbers of 238868, 240674, 246524, and 243840 were used for the numerical model for the rectangular grooved channel, rectangular-triangular hybrid grooved channel, rectangular-trapezoidal hybrid grooved channel, and rectangular-circular hybrid grooved channel, respectively. Figure 3 shows the changes of Nu and friction factor with the element numbers at Re = 10000 for the rectangular wavy channel.

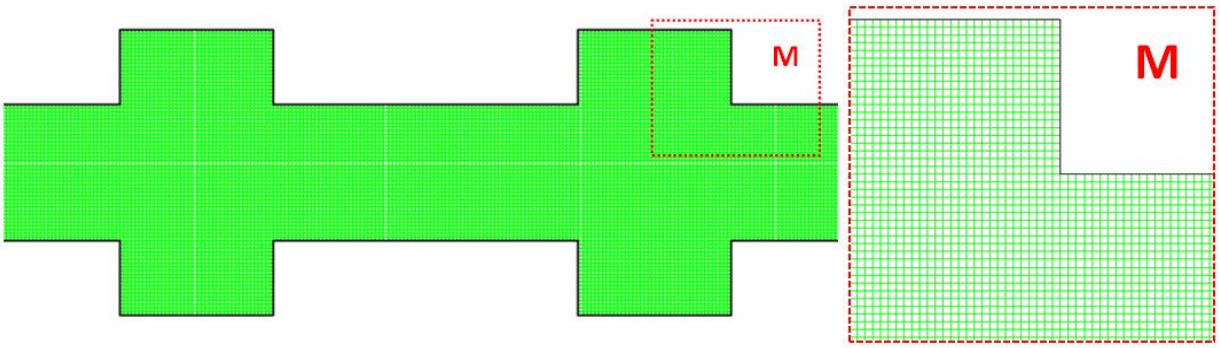

Figure 2. Element structure of the numerical model with detail (for rectangular channel)

The numerical solutions were carried out with ANSYS Fluent version 15.0, which is Computational Fluid Dynamics (CFD) software. The second order upwind approach was utilized to discretize the equations. The relationship between velocity and pressure was assessed with the SIMPLE algorithm. Zontul et al. [40] reported that there was a fine agreement

between the numerical results acquired using the standard k-ε turbulence approach and the experimental results. For this reason, the standard k-ε turbulence approach was preferred as the flow model in this study.

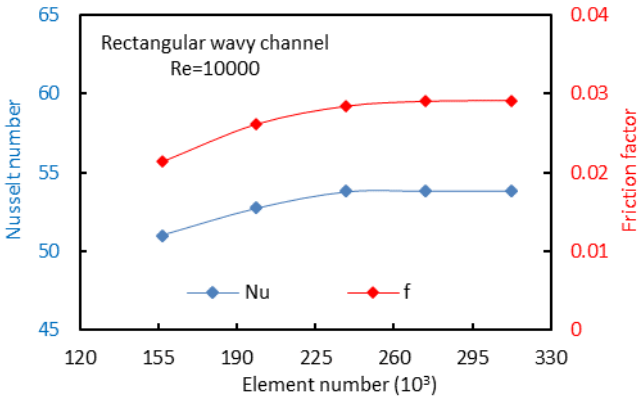

Figure 3. Mesh independence testing

As the convergence criterion, 10^{-8} were set in the energy equations and 10^{-5} in the other equations. Some initial and boundary conditions were utilized in the model for numerical solutions. In all corrugated channels, the fluid entered the duct with an average velocity of u_{in} and a constant temperature of T_{in} = 300 K.

- $u_i = u_{in}, u_j = 0, T = T_{in} = 300\ K$, in the channel inlet

  No-slip and adiabatic conditions were defined for the straight sections (L_1 and L_3) at the inlet and exit of the duct.

- $u_i = u_j = 0, \frac{\partial T}{\partial y} = 0,$ the straight lengths at the inlet and exit of the duct.

  The lower and upper wavy surfaces of the channel (L_2) were maintained at a constant temperature of T_w = 380 K.

- $u_i = u_j = 0, T = T_w = 380\ K$, in the wavy channel surface

  At the channel outlet, the pressure outlet condition was used.

- $\frac{\partial u_i}{\partial x} = 0,\ \frac{\partial u_j}{\partial x} = 0,\ \frac{\partial T}{\partial n} = 0$, in the channel outlet

  The boundary conditions applied to the computational area in the numerical model are shown in Figure 4.

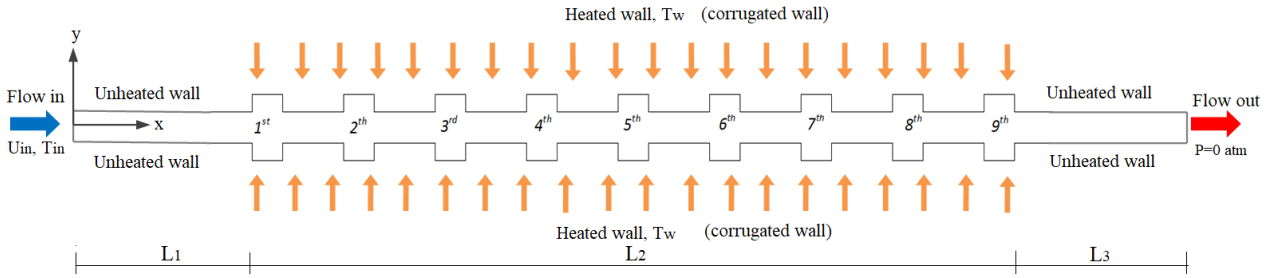

Figure 4. Description of the boundary conditions

2.4 Validation of Numerical Solutions

To determine the validity of numerical solutions, the results of the present study were compared and validated with the results of previous numerical and experimental studies. For straight duct and rectangular wavy duct, Nusselt numbers and friction factor values obtained in this study were compared with the numerical and experimental results of Zontul et al. [40] (see for detail, Akcay [58]). Dittus-Boelter correlation (Eq. (8)) is widely used to determine the Nusselt number in straight channels, and Petuklov correlation (Eq. (9)) is used to calculate the friction factor [59]. In addition, in this study, the Nu and *f* values obtained for the straight channel were compared with empirical relations. The comparison of numerical solutions with previous study results is given in Figure 5.

The Dittus-Boelter correlation is given by Eq. (8):

$$Nu = 0.023 Re^{0.8} Pr^{0.4} \tag{8}$$

The Petuklov correlation is calculated by Eq. (9):

$$f = [0.79 \ln(Re) - 1.64]^{-2} \tag{9}$$

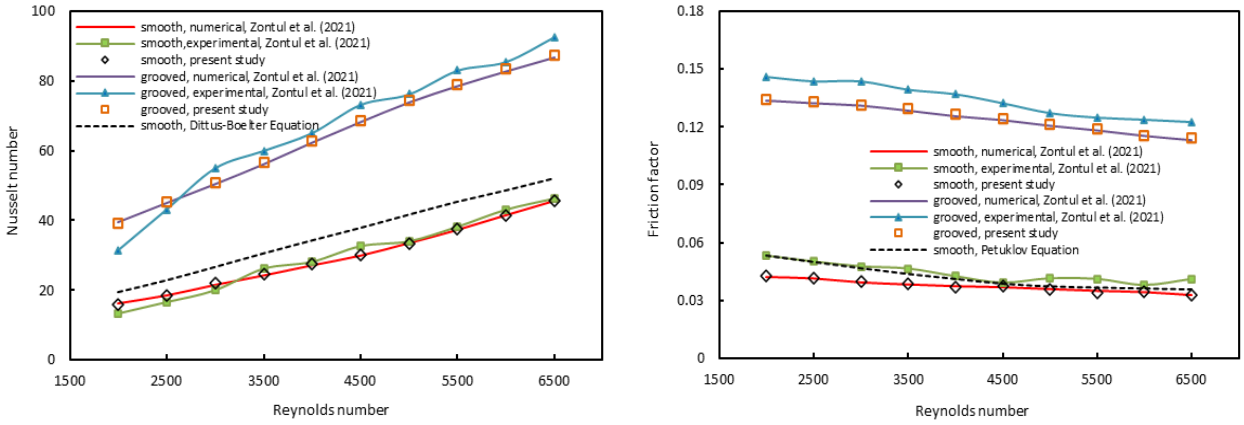

(a) (b)

Figure 5. Validation of this study with previous works: (a) Nu with Re and (b) *f* with Re

2.5 Data Reduction

In this study, the channel inlet velocity was determined by the Re calculated based on the hydraulic diameter, D_h. The Reynolds number varied in the range of $2000 \leq Re \leq 10000$. Hydraulic diameter and Reynolds number were calculated using Eqs. (10) and (11), respectively [58].

$$D_h = H_{min} + H_{max} \tag{10}$$

$$Re = \frac{\rho u_{in} D_h}{\mu} \tag{11}$$

where, ρ, u_{in}, and μ show density of fluid, inlet velocity, and dynamic viscosity, respectively.

The heat transfer achieved in the duct was evaluated by the Nusselt number. The average Nusselt number, Nu_{ave} was calculated with Eq. (12) [40].

$$Nu_{ave} = \frac{h\, D_h}{\lambda} \tag{12}$$

where, h is the convection heat transfer coefficient, and λ is the thermal conductivity coefficient.

The convection heat transfer coefficient, h is given by [59].

$$h = \frac{q''}{\Delta T_{ln}} \tag{13}$$

where, ΔT_{ln} is the logarithmic temperature difference, and q'' shows heat flux.

The logarithmic temperature difference is found as shown in Eq. (14) [59]:

$$\Delta T_{ln} = \frac{(T_o - T_{in})}{ln\left(\frac{T_w - T_{in}}{T_w - T_o}\right)} \tag{14}$$

where, T_{in}, T_o, and T_w are the inlet and outlet temperatures of the water and the temperature of the grooved surfaces, respectively.

The thermal enhancement rate is calculated in two different ways by taking the straight channel and the rectangular wavy channel as reference. TE_s and TE_w are the thermal enhancement rates obtained by taking the straight channel and rectangular wavy channel as reference, respectively [33]:

$$TE_s = \frac{Nu_w}{Nu_s} \tag{15}$$

$$TE_w = \frac{Nu_h}{Nu_{rec}} \tag{16}$$

where, Nu_w, Nu_s, Nu_h, and Nu_{rec} refer to the Nusselt number obtained in all grooved channels, the Nusselt number obtained in the straight duct, the Nusselt number obtained in hybrid grooved channels, and the Nusselt number obtained only in the rectangular wavy channel, respectively.

The friction factor, *f* is calculated by using the equation below [40]:

$$f = \frac{2\Delta P D_h}{\rho L u_{in}^2} \tag{17}$$

$$\Delta P = P_{out} - P_{in} \tag{18}$$

The relative friction factor was calculated in two different ways by using the straight channel and the rectangular wavy channel as reference. $(f_{rel})_s$ and $(f_{rel})_w$ show the relative friction factors obtained by taking the straight channel and rectangular wavy channel as reference, respectively [58]:

$$(f_{rel})_s = \frac{f_w}{f_s} \tag{19}$$

$$(f_{rel})_w = \frac{f_h}{f_{rec}} \tag{20}$$

where, $(f_{rel})_w$, $(f_{rel})_s$, $(f_{rel})_h$ and $(f_{rel})_{rec}$ refer to the friction factor obtained in all wavy channels, the friction factor obtained in the flat duct, the friction factor obtained in hybrid wavy channels, and the friction factor obtained only in the rectangular wavy channel, respectively.

Wavy channels increase heat transfer, but they also cause an increase in pressure drop inside the channel. Therefore, the performance factor, *PF* in the channel is found by taking the ratio of the heat transfer increase to the friction factor. Eq. (21) shows the performance factor, PF_s calculated using straight channels as reference. Eq. (22) shows the performance factor, PF_w calculated by taking the rectangular wavy channel as reference [33]:

$$PF_s = (Nu_w/Nu_s)\,(f_w/f_s)^{-1/3} \tag{21}$$

$$PF_w = (Nu_h/Nu_{rec})\,(f_h/f_{rec})^{-1/3} \tag{22}$$

If the performance factor exceeds 1, it shows that the increase in heat transfer is greater than the friction factor. If the performance factor is below 1, it means that the friction in the channel is higher than the heat transfer. In research studies, it is aimed that the *PF* value is above 1 [58]. In this study, the performance factor was calculated based on two different reference values.

3. RESULTS AND DISCUSSION

In this section, images of velocity, temperature, pressure and vorticity contours were obtained at different Reynolds numbers in order to observe the impacts of hybrid channel profiles on flow and heat transfer. The numerical findings were compared with the rectangular groove duct. Nusselt number, thermal enhancement rate, friction factor, and performance factor were obtained for all channel flows, and the results were plotted graphically.

3.1 Effects on Flow and Heat Transfer of Hybrid Groove Profile

In Figure 6, images of velocity contours and temperature contours at Re = 2000 are presented for all wavy channel configurations. The images given belong to the 5th, 6th and 7th grooves in the upstream. As seen in Figure 6(a), while the main flow goes parallel to the surface along the channel, flow loops occur in groove gaps. These loops seem to completely cover the wavy cavities. Since the triangular groove has the lowest surface area compared to the other groove profiles, the flow loop in the triangular cavity is smaller. These flow loops transport the colder fluid in the channel center to the hot groove surfaces. The contact of hot surfaces with cold fluid induces the temperature of corrugated walls to decrease. In Figure 6(b), it can be seen that the wavy cavities are covered with hot fluid for all channel flows. Especially in rectangular wavy cavities, the temperature gradient is higher than other wave profiles. Lower surface temperature has occurred in hybrid wave profiles. It is observed that for each wavy cavity, the temperature gradient is lower where the flow loops begin and higher where the flow loops end. It has been determined that the surface temperature in the triangular groove is lower than in other profiles. This may have been due to the fact that the flow loops completely covered the surface because of the low surface area.

In Figure 7, images of velocity contours and temperature contours at Re = 10000 are given for all wave profiles. The images presented in the figure belong to the 5th, 6th, and 7th wave profiles in the upstream. As seen in Figure 7(a), higher mass flow rate was provided by increasing the inlet velocity. In addition, increasing inertial forces within the channel caused the flow loops occurring in wavy cavities to grow. These loops completely surrounded the wavy spaces. Flow loops are important phenomena in terms of heat transfer because they improve the flow mixing and create a homogeneous flow structure. As seen in Figure 7(b), the temperature of the corrugated walls decreases considerably compared to Figure 6(b) for all grooved ducts. The rectangular wavy profile has the highest temperature gradient. It was observed that the surface temperatures in the hybrid channels were lower than the surface temperature of the rectangular grooved duct. Figures 6 and 7 reveal that the shape of the duct profile and the Re significantly affect the heat transfer and flow behavior.

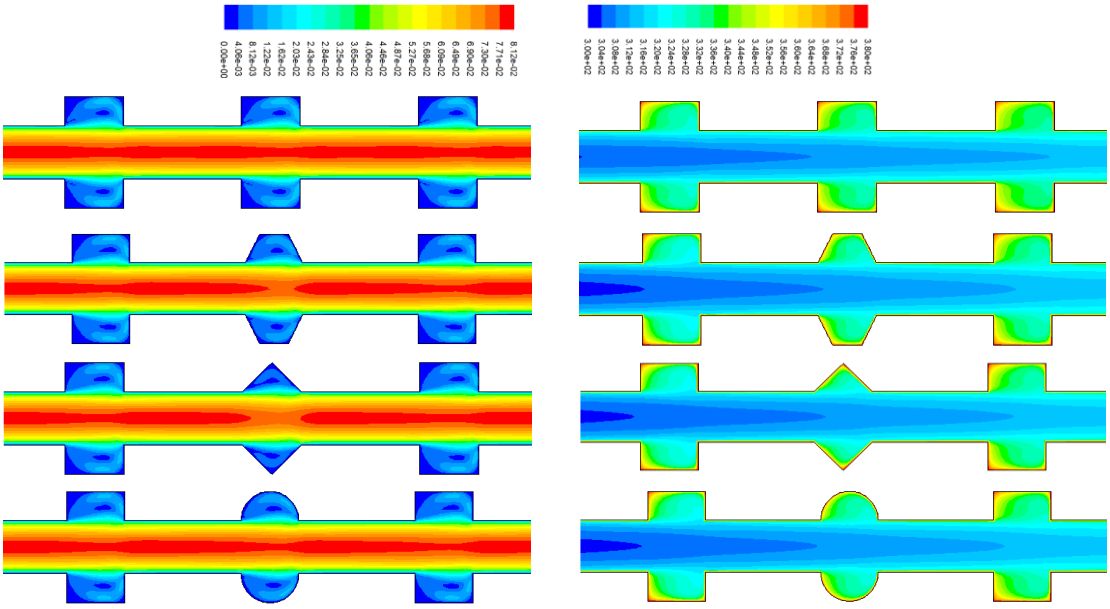

(a) (b)

Figure 6. Images of: (a) velocity and (b) temperature contours at Re = 2000 for all channel flows

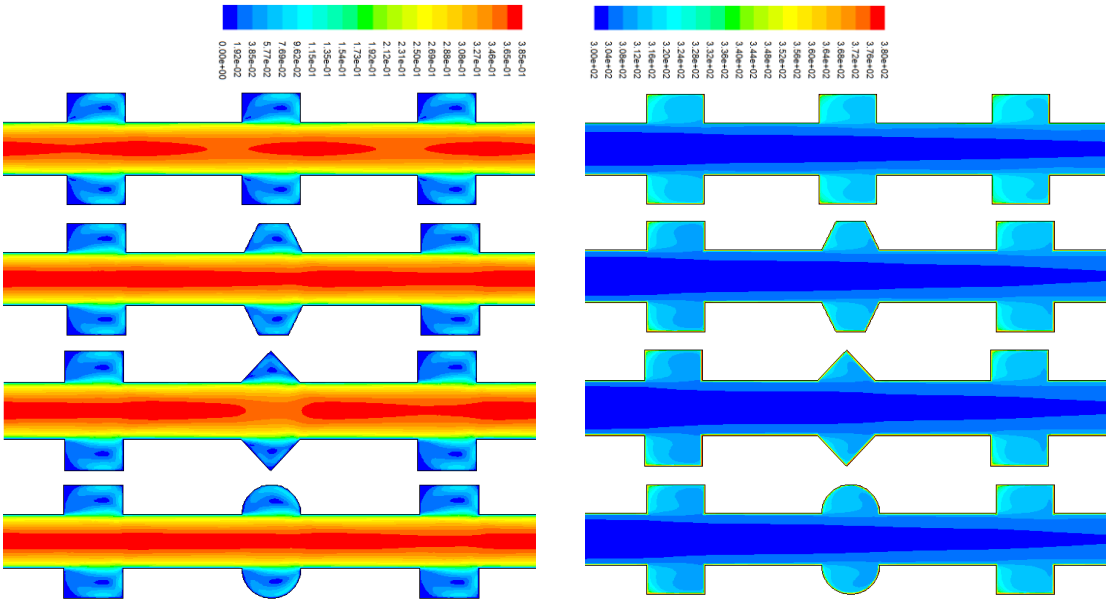

(a) (b)

Figure 7. Images of: (a) velocity and (b) temperature contours at Re =10000 for all channel flows

Figure 9 shows the images of vorticity magnitudes at Re = 10000 for all wavy channels. The images belong to 4th, 5th, and 6th wave profiles. Vorticity lines continue horizontally in all channels. At the beginning of the wavy profiles, the lines intensify and then spread into the cavities. The presence of lines along the wavy surface is observed in all profiles except rectangular profiles. In rectangular profiles, vorticity lines are observed only on the right and upper walls of the cavity. The reason for this is that the flow in the cavity reverses and completely covers the wavy surface in hybrid wave profiles, while the flow loop in the cavity cannot reach the left edge of the cavity in rectangular profiles. Among the hybrid wave profiles, the vorticity magnitudes of the rectangular-circular and the rectangular-trapezoidal profiles are quite similar since the surface areas of these profiles are close to each other.

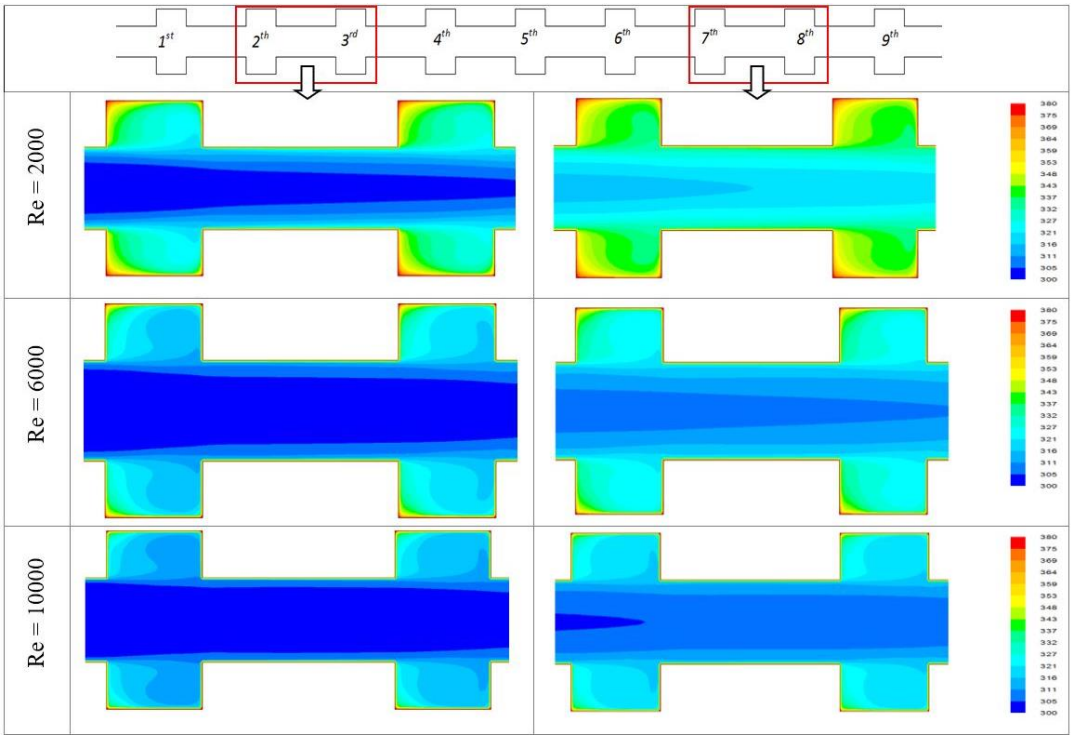

(a)

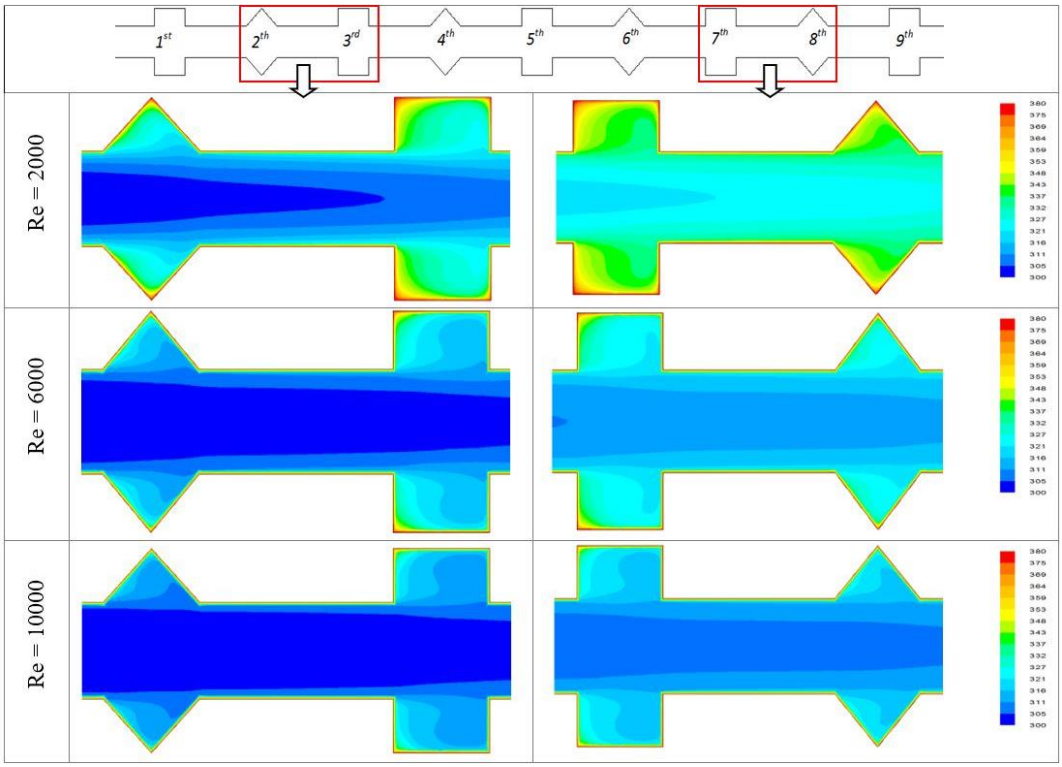

(b)

Figure 8. Images of temperature contours at different Reynolds numbers for all wavy channels: (a) rectangular, (b) rectangular-triangular hybrid;

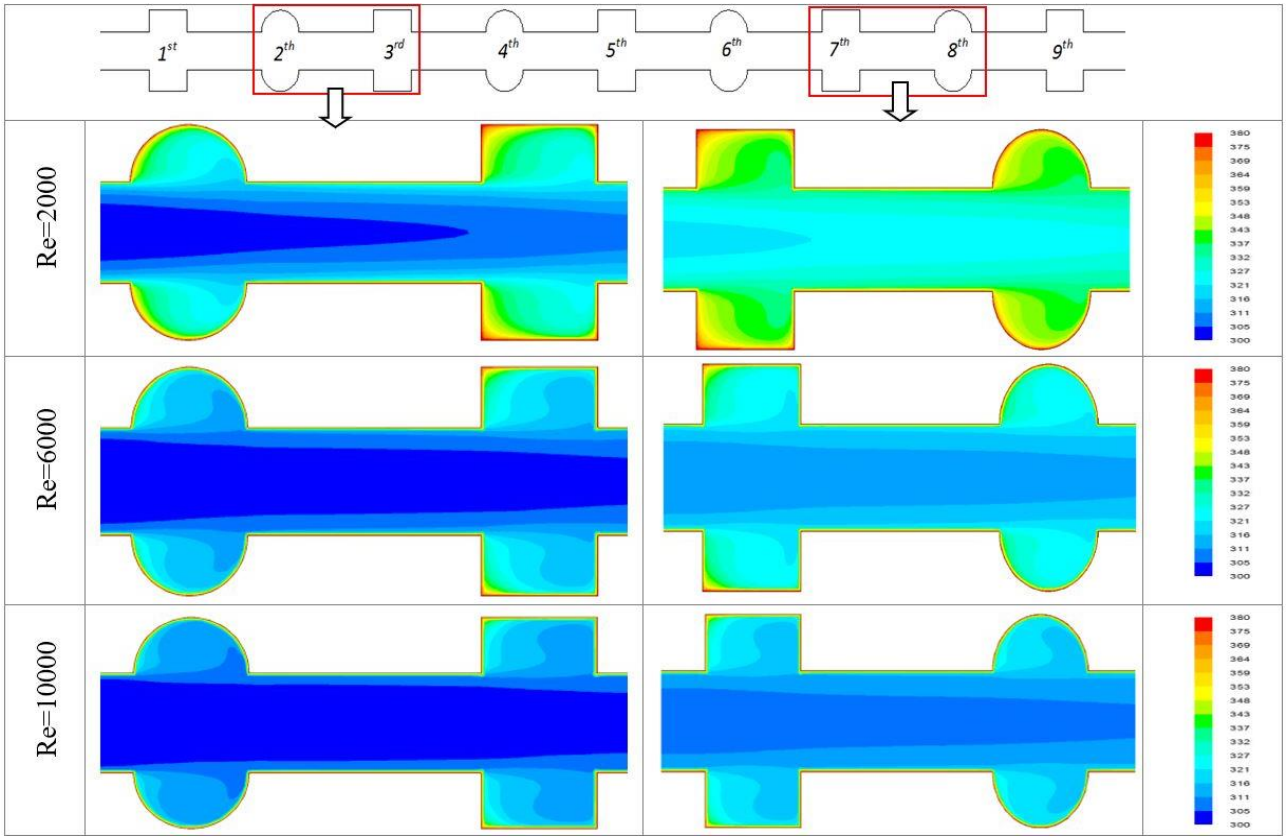

(c)

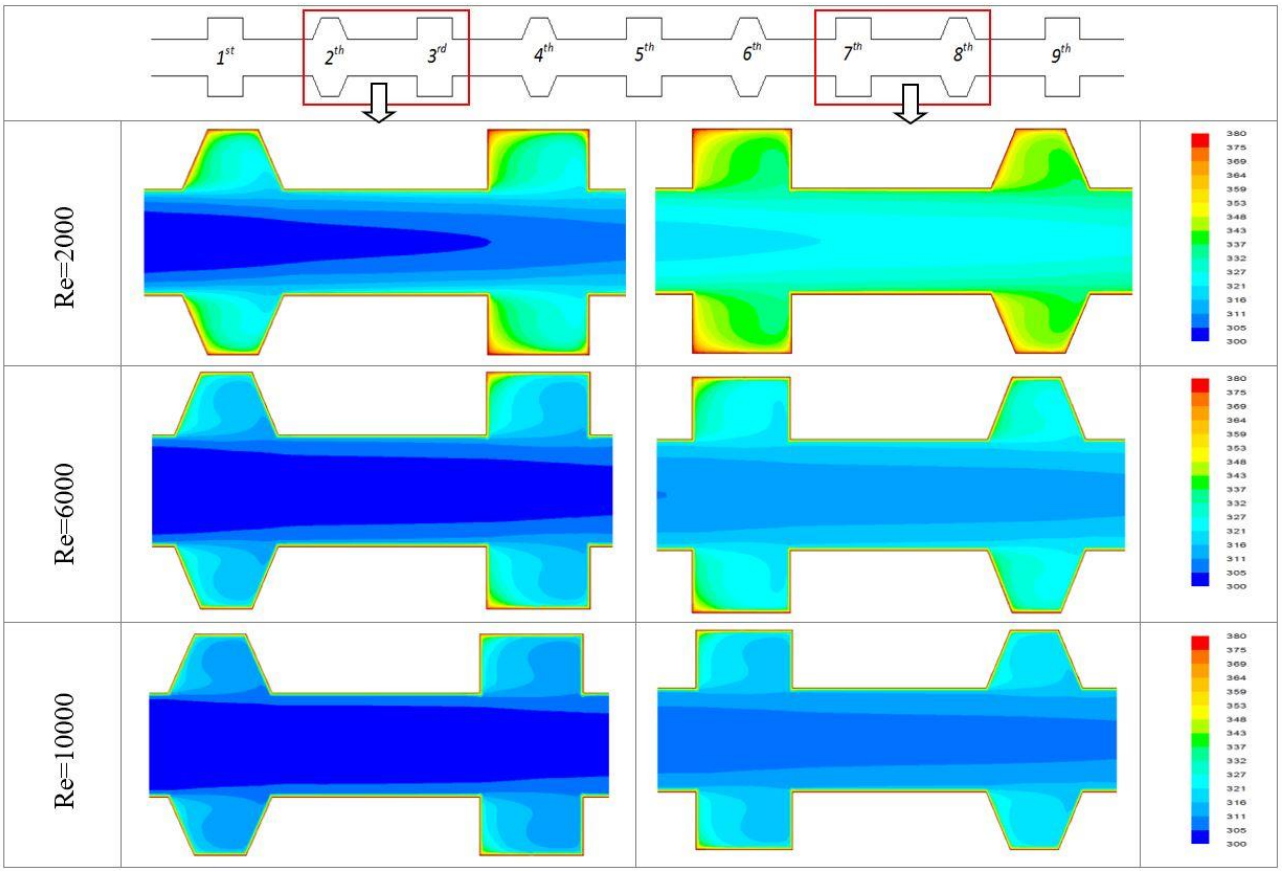

(d)

Figure 8. (cont.) (c) rectangular-circular hybrid and (d) rectangular-trapezoidal hybrid

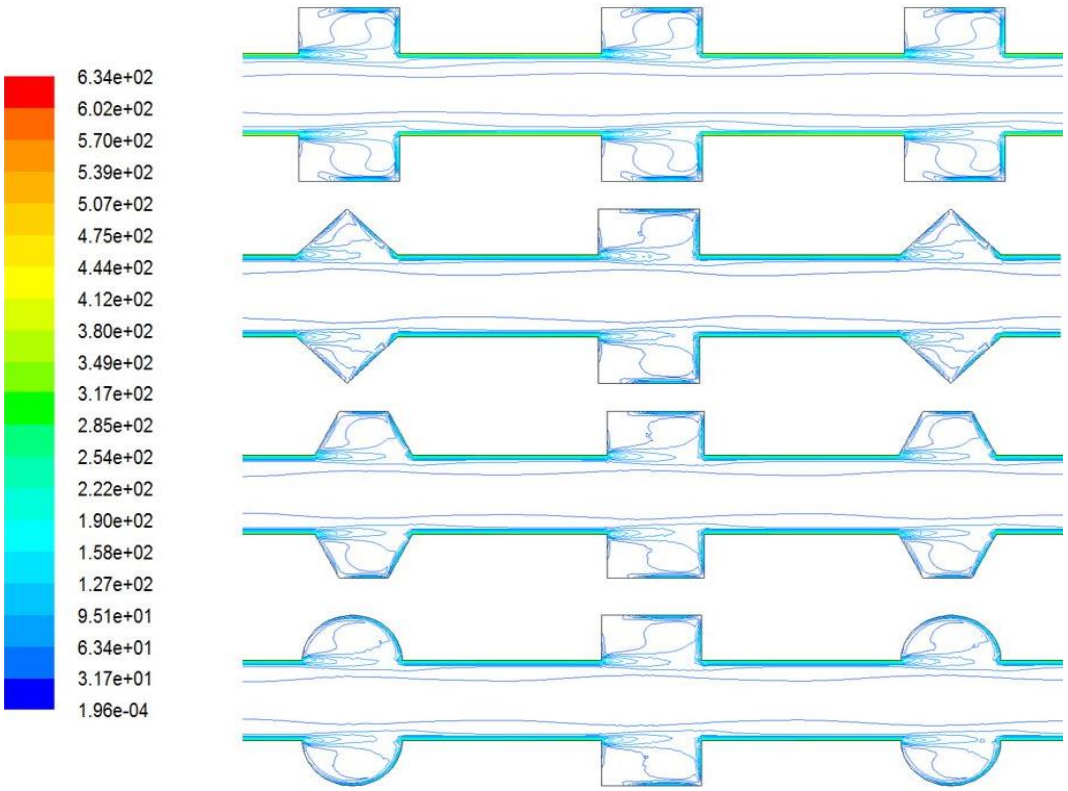

Figure 9. Images of vorticity contours for all wavy channels at Re = 8000

In Figures 10 to 12, the velocity vectors of the 5th and 6th wave profiles in the flow direction of the hybrid wave channels are given for Re = 8000. The image of the velocity vectors of the rectangular-triangular hybrid wavy channel is seen in Figure 10. The 5th wave profile is rectangular, while the 6th wave profile is triangular. It is seen that in both wave profiles, the main flow velocity vectors flow in the upward direction and parallel to each other. When it comes to wavy cavities, the direction of the velocity vectors changes and is directed towards the wave cavities (downstream). From the right edge of the cavities, a large flow loop is formed along the wavy surface. The flow loop formed in a rectangular cavity is closer to the right edge of the cavity, and velocity vectors near the left edge are smaller in size. In the triangular cavity, the flow loop is in the middle of the cavity, and the velocity vectors are closer in terms of size. Because the surface area of the triangular wave profile is smaller than the rectangular profile, the magnitudes of the vectors are less affected along the flow. In the rectangular groove with a larger surface area, the size of the vectors that cannot participate in the flow loop becomes smaller due to the decrease in velocity. In the rectangular groove, the flow mixing is better in the region close to the right edge, while it is not good in the region close to the left edge. In the triangular groove, the flow affects both sides homogeneously.

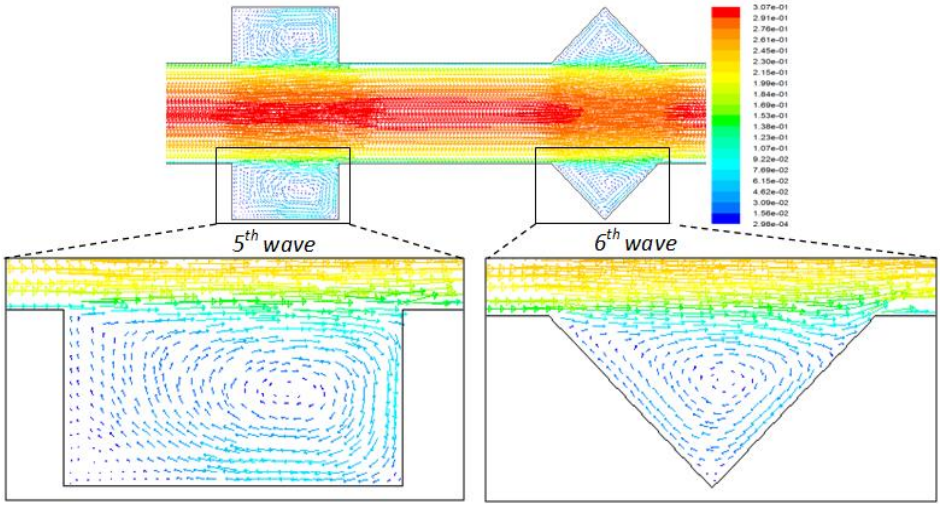

Figure 10. Image of velocity vectors for rectangular-triangular hybrid wavy channels at Re = 8000

The image of the velocity vectors of the rectangular-circular hybrid wavy channel for Re = 8000 is given in Figure 11. As seen, the 5th wave profile has a rectangular shape, while the 6th wave profile has a circular shape. The main

flow vectors are parallel to each other in the channel, while the magnitude and direction of the vectors change in the wavy cavities. The structures of the vectors formed in the rectangular cavity are shown in Figure 8(a). In the circular cavity, velocity vectors leaving the main flow create a large flow loop in the middle of the cavity by moving in the opposite direction parallel to the wavy surface. The magnitudes of the vectors near the right edge of the cavity are larger than the magnitudes of the vectors at the left edge because these vectors have just separated from the main flow and their speeds are higher. Due to the slowing down of the flow velocity, the magnitudes of the vectors decreased in the region near the left surface of the cavity.

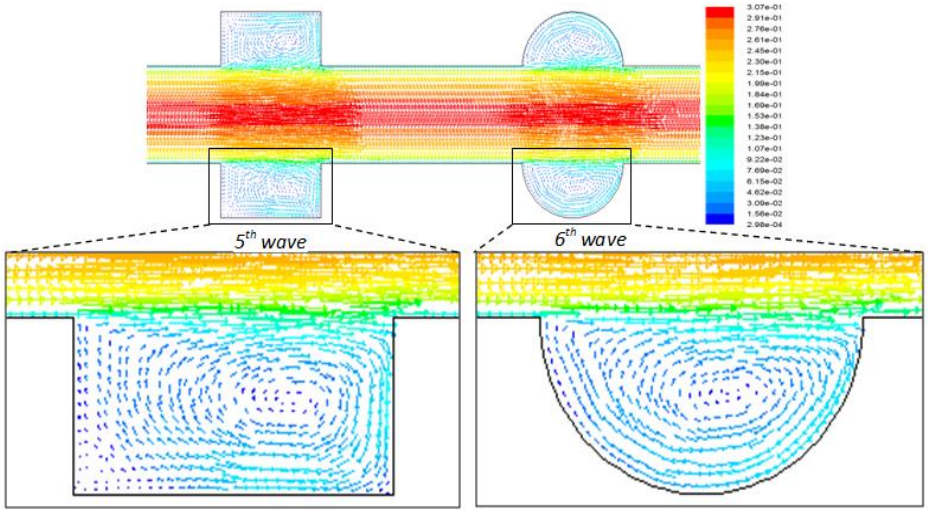

Figure 11. Image of velocity vectors for rectangular-circular hybrid wavy channels at Re = 8000

Figure 12 shows the image of the velocity vectors of the rectangular-trapezoidal hybrid wavy channel for Re = 8000. The 5th wave has a rectangular profile, while the 6th wave has a trapezoidal profile. The structures of the vectors formed in the rectangular cavity are similar to the situation in the rectangular profiles presented in Figures 10 and 11. In the trapezoidal cavity, the velocity vectors separated from the main flow continue parallel along the trapezoidal surface in the opposite direction (downstream). A large flow loop occurs in the middle of the cavity (slightly near the right). The magnitude of the vectors near the left edge of the groove is slightly smaller than that at the right edge because the velocity of the fluid in the region near the left edge of the groove has decreased, and therefore the size of the vectors has decreased.

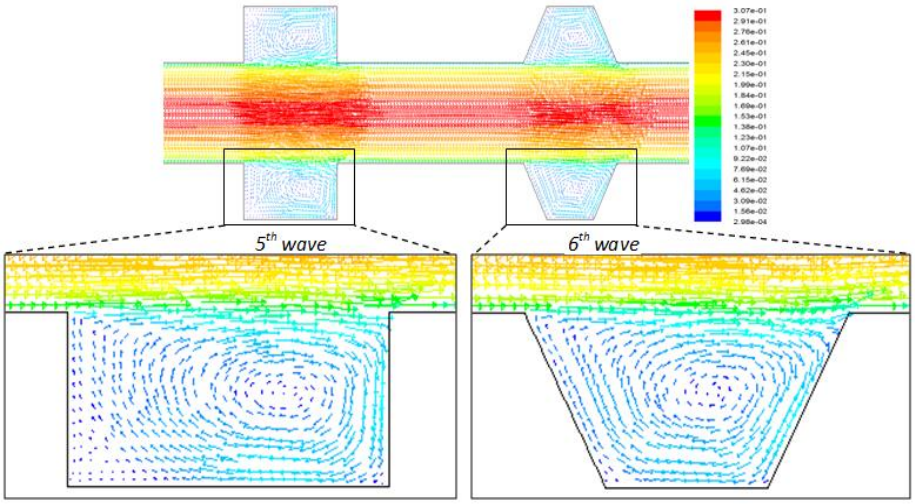

Figure 12. Image of velocity vectors for rectangular-trapezoidal hybrid wavy channels at Re = 8000

Figure 13 shows the local surface heat transfer coefficients along the lower wavy walls of all studied wavy profiles for Re = 6000. The heat transfer coefficient continues as a straight line on the straight walls connecting the wavy grooves, and there are fluctuations in the grooves due to the cross-section expansion. The heat transfer coefficient of the rectangular groove duct is quite low compared to other hybrid groove profiles. The heat transfer coefficient of the rectangular-triangular groove duct is slightly lower than other hybrid wave profiles. It is seen that the values of rectangular-circular and rectangular-trapezoidal groove ducts are very close to each other.

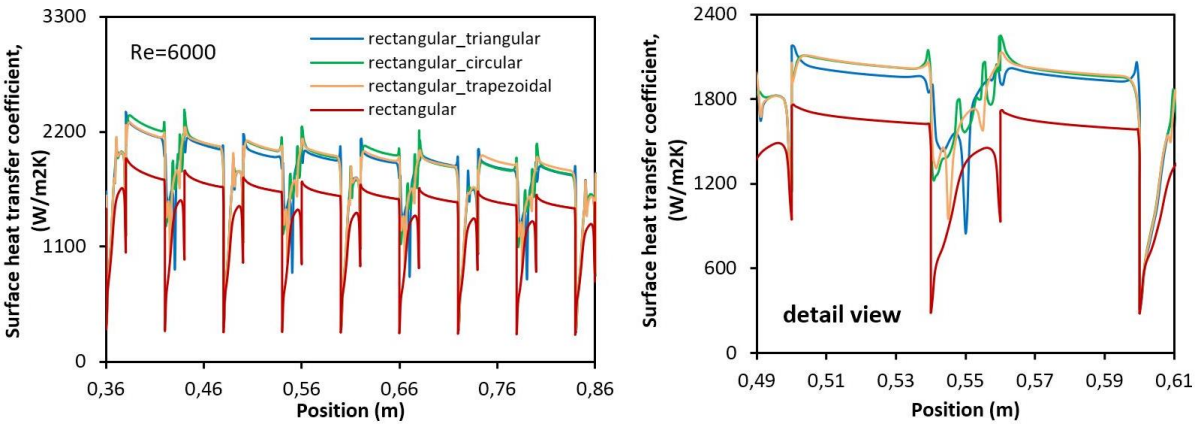

(a) (b)

Figure 13. (a) Local surface heat transfer coefficient for all grooved ducts at Re = 6000 and (b) detail view

Figure 13(a) shows the average Nusselt number (Nu) by Reynolds number (RE). Nu increases as Re increases. Compared to straight channels, the Nusselt number obtained in grooved channels is quite high. It is seen that the Nu is higher in hybrid grooved channels than in rectangular grooved channels. When hybrid grooved channels are compared among themselves, it is observed that the Nusselt numbers obtained in rectangular-trapezoidal and rectangular-circular grooved ducts are quite close to each other, and they are higher than Nusselt numbers obtained in the rectangular-triangular wave profile. In the context of the study, since the surface area of the triangular geometry was smaller among the hybrid groove profiles, a lower Nusselt number was found compared to other hybrid groove profiles. Because the surface area of circular and trapezoidal geometries was quite close to each other, the Nusselt number was found to be quite similar. The highest Nusselt number was found as 64.43 in the rectangular-trapezoidal hybrid profile at Re = 10000. This was followed by rectangular-circular hybrid profile (Nu=64.30), rectangular-triangular hybrid profile (Nu=62.13), rectangular wave profile (53.81), and straight channel (16.20), respectively. The use of the hybrid wave profile in channel flows enabled higher Nusselt values to be obtained compared to the uniform wave profile.

Figure 14 shows the local surface heat transfer coefficients along the lower wavy walls with different Reynolds numbers for the rectangular-trapezoidal hybrid wavy channel. It is seen that surface heat transfer coefficients are significantly affected by Re. Heat transfer coefficients increase as Re increases. While the difference between the heat transfer coefficient is higher between Re = 2000 and Re = 6000, this difference is smaller between Re = 6000 and Re =10000.

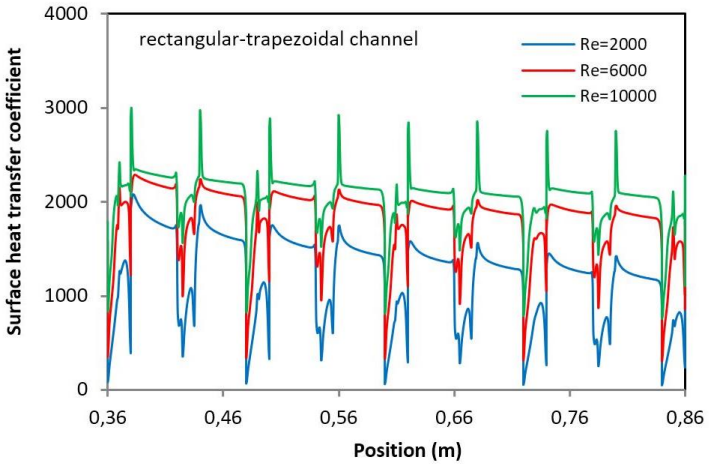

Figure 14. Local surface heat coefficient with Re in the rectangular-trapezoidal hybrid corrugated channel

Figure 15(b) indicates the variation of thermal enhancement rate by Reynolds number. The straight channel is considered as a reference. In the context of the study, it was determined that there was an increase in heat transfer in other ducts compared to the flat duct. In all groove ducts, the thermal enhancement rates were significantly higher than the rate in the flat duct. In all wavy channels, thermal enhancement rate tended to increase up to Re ≤ 8000. However, it showed a decreasing trend after Re = 8000 because the Nusselt number was found to be higher at high Reynolds numbers in the flat duct. The thermal enhancement rate showed similar characteristics in rectangular-trapezoidal and rectangular-circular hybrid profiles. TE was higher in hybrid profiles compared to rectangular groove duct flow. The highest TE (4.39) was obtained in the rectangular-circular hybrid profile at Re = 8000. This was followed by rectangular-trapezoidal hybrid profile, rectangular-triangle hybrid profile, and rectangular wave profile (Nu = 4.37, Nu = 4.24, and Nu = 3.64), respectively.

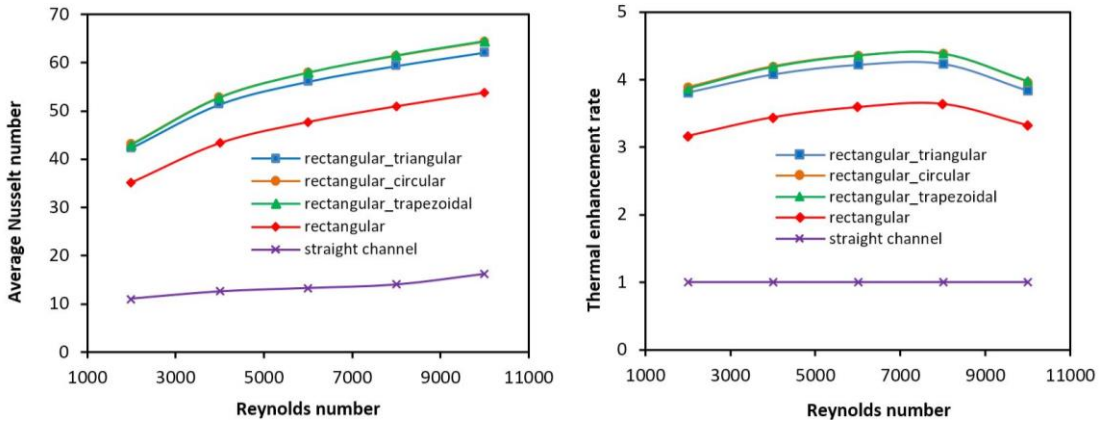

(a) (b)

Figure 15. (a) Average Nusselt number and (b) Thermal enhancement rate by Re for all channel flows

3.2 Effects on pressure drop and friction factor of hybrid groove profiles

In Figure 16, contour images of the pressure changes along all the wavy channels for Re=2000 and Re=10000 are given. It is observed that the pressure drop along the corrugated ducts increases for both Re values. On the other hand, it is not seen that there is a significant difference in the pressure contours along the corrugated ducts at Re = 2000. The pressure drop at Re = 10000 is higher than the pressure drop at Re = 2000. However, the change in wave profiles did not cause a significant change in the pressure contours.

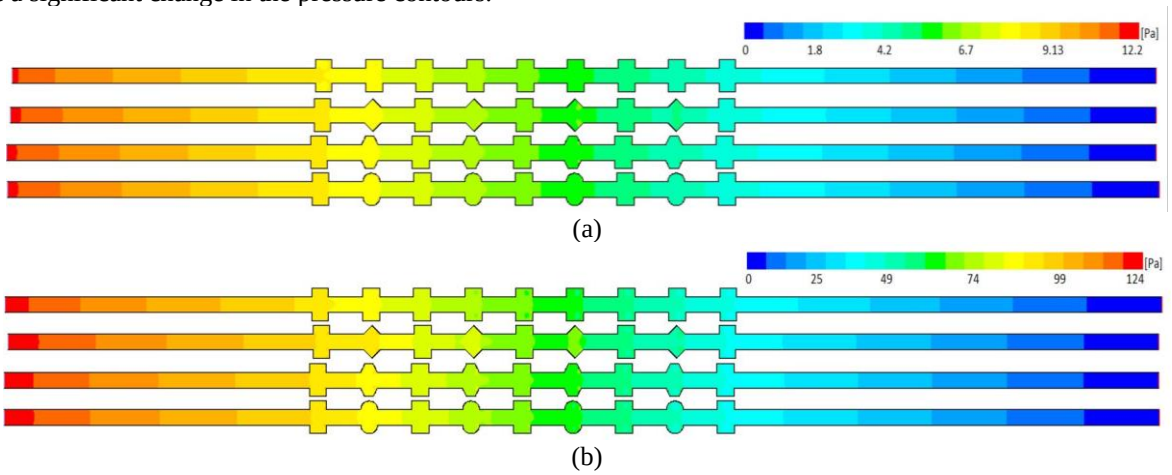

(a)

(b)

Figure 16. The total pressure images for all wavy channel flows: (a) Re = 2000 and (b) Re = 10000

Figure 17 presents the variation of local surface friction coefficients along the examined wavy surfaces at Re = 4000 for all wavy channels. It is seen that surface friction coefficients are not much affected by wave profiles. Similar surface friction coefficients were obtained for all wave profiles. While the structure of the wave profiles affected the heat transfer coefficient positively (Figure 13(a)), it hardly changed the friction factor. This result reveals that there is an improvement in heat transfer in hybrid wavy channels while the friction factor remains the same for the same Reynolds number. This result is very important for duct designers since higher heat transfer improvement is achieved with unchanged pumping costs.

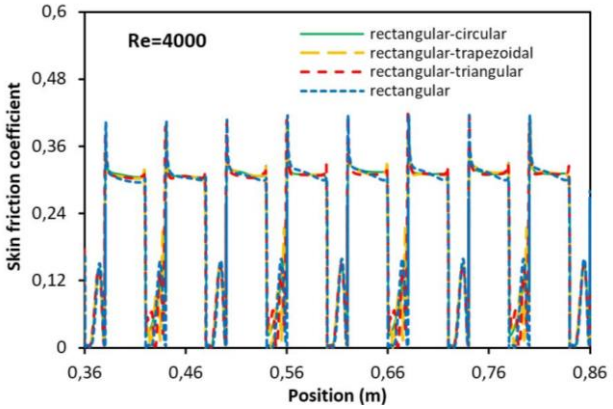

Figure 17. Variation of local surface friction coefficient in all wavy channels for Re = 4000

Figure 18 shows the surface friction coefficients along the lower wavy walls for different Reynolds numbers in the rectangular-circular hybrid wavy channel. It is seen that surface friction coefficients are highly affected by Reynolds number. In the context of the study, it was determined that frictions occurring along wavy surfaces increased as Reynolds numbers increased. While very low surface friction occurred at Re = 2000, these friction values increased at Re = 10000. As seen in the figure, especially at Re = 6000 and Re = 10000, the curves continue to rise along the corrugated surfaces, then form a small peak and continue with straighter lines between the two grooves.

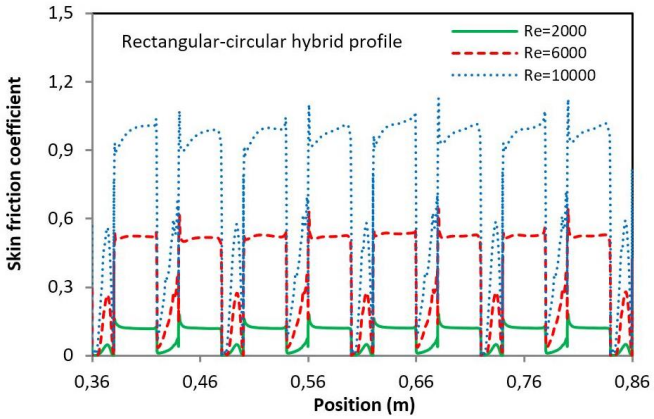

Figure 18. Variation of local surface friction coefficient with different Re in the rectangular-circular hybrid profile

The variation of pressure drop by Reynolds number is presented in Figure 19(a). For all channel flows, as the Re increased, the pressure drop also increased dramatically. The pressure drop was higher in wavy channels than in straight channels. Interestingly, the shape of the wave profile had little impact on the pressure drop. Whereas almost the same pressure drop was obtained in all wave profiles for Re ≤ 6000, a slight difference occurred after Re ≥ 6000. The pressure drop in hybrid wave profiles increased slightly at higher Reynolds numbers compared to the rectangular wave profile. Here, the main purpose is to provide high heat transfer with low-pressure drop in channel flows. In the literature, it has been reported that high heat transfer is achieved in wavy channels, but there is a significant increase in pressure drop [33, 40, 58]. In the present study, in hybrid wavy channels, higher heat transfer was achieved compared to the uniform wave profile, but there was no significant increase in pressure drop. The highest-pressure drop was seen in the rectangular-triangular wave profile of 62.15 Pa at Re = 1000, and it was followed by the rectangular-trapezoidal wave profile (61.18 Pa), rectangular-circular wave profile (61.06 Pa), rectangular wave profile (59.42 Pa), and straight channel flow (17.21 Pa). Figure 19(b) shows the friction factor by the Reynolds number. The friction factor was calculated taking into account the pressure drop. It is seen that the friction factor in all wavy channels is higher than in the straight channel and decreases as the Reynolds number decreases. The friction factor in hybrid wavy channels is very close to each other and is slightly higher than the rectangular wavy channel.

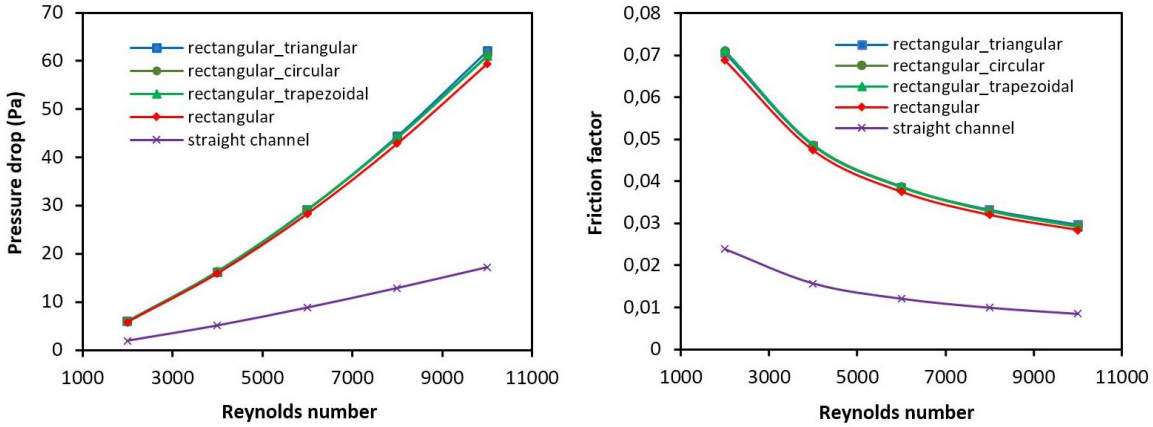

(a) (b)

Figure 19. (a) Pressure drop and (b) Friction factor by Re for all channel flows

3.3 Effects on Performance Factor of Hybrid Wavy Profiles

Figure 20(a) shows the performance factor calculated by taking the straight channel as reference, and Figure 20(b) shows the performance factor obtained by taking the rectangular wavy channel as reference. A performance factor above the reference value indicates that the thermal enhancement rate in the duct is greater than the resulting pressure drop. This is a desirable condition. If the performance factor falls below the reference value, it shows that the friction losses in the duct are higher than the heat transfer. As seen in Figure 20(a), in the context of this study, PF_s values far above the reference value were obtained for all studied wavy channels. While PF_s values tended to increase in the range of 2000 ≤

Re ≤ 8000, they tended to decrease after Re ≥ 8000. The reason for this is that the thermal enhancement rate increases in the range of 2000 ≤ Re ≤ 8000 and then tends to decrease. In the case of rectangular-circular and rectangular-trapezoidal hybrid profiles, the thermal enhancement rates were obtained at close values. This also caused the PF_s values to be close to each other. The highest PF_s value was found to be 2.63 in the rectangular-circular hybrid profile at Re = 8000. This was followed by rectangular-trapezoidal hybrid profile (2.62), rectangular-triangular hybrid profile (2.52), and rectangular wave profile (2.22), respectively. Figure 6a shows that by using the hybrid wave profile in channel flows, PF_s values of more than 2.6 times can be obtained compared to straight channels. When the rectangular wavy channel was taken as reference (Figure 20(b)), it was observed that the PF_w values of all hybrids corrugated channels exceeded the reference value, and they decreased as Re value increased. The reason for these decreases is that the increase in thermal enhancement rate is less at increasing Reynolds numbers and the increase in pressure drop is greater. The highest PF_w value was calculated as 1.22 in the rectangular-circular hybrid profile at Re = 2000. This was followed by rectangular-trapezoidal profile (1.21) and rectangular-triangular profile (1.19), respectively. As seen in Figure 20(b), it is possible to increase PF_w values by more than 20 % if a hybrid wave profile is used instead of a uniform wave profile in channel flows.

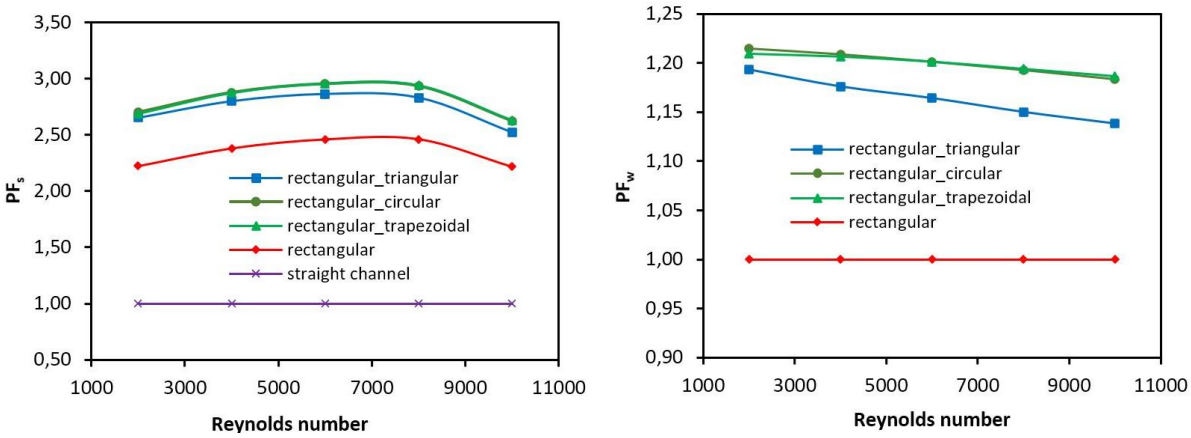

(a) (b)

Figure 20. Variation of performance factor by Re: (a) the straight channel is taken as reference and (b) the rectangular wavy channel is taken as reference

4. CONCLUSIONS

In this study, the hydraulic and thermal characteristics of wavy channels with hybrid profiles were examined at different Reynolds numbers (2000 ≤ Re ≤ 10000). The hybrid wavy channel includes separate combinations of a rectangular wave profile with triangular, trapezoidal, and circular groove profiles. The obtained results were compared with rectangular grooved duct and flat duct flows. Images of flow and temperature contours at different Reynolds numbers were obtained for all wavy channels. The important findings of the study are presented below:

i) Rectangular-circular and rectangular-trapezoidal hybrid channels showed similar behavior in terms of hydraulic and thermal enhancement. It was observed that large flow loops occurred in wave cavities in all wavy channels. While these flow loops were in the middle of the cavity in circular, trapezoidal, and triangular profiles, they were close to the right edge of the cavity in the rectangular profile.

ii) All wavy channels had higher pressure drop and heat transfer compared to the straight channel. Hybrid grooved channels, on the other hand, provided higher heat transfer without a significant increase in pressure drop compared to the rectangular grooved channel. The pressure drops in all hybrid wavy channels showed similar behavior and were found to be slightly higher than the rectangular grooved duct.

iii) The highest Nusselt number Nu = 64.68 was obtained in the rectangular-trapezoidal grooved hybrid duct at Re =10000. The heat transfer in the rectangular-circular grooved hybrid channel improved by 2.22 times at Re = 10000 compared to the flat duct. It was determined that heat transfer in rectangular-circular and rectangular-trapezoidal hybrid groove profiles improved 4.38 times compared to straight ducts at Re = 8000 and 1.23 times compared to rectangular corrugated ducts at Re = 2000.

iv) The performance factor in hybrid wavy channels was quite high compared to rectangular and straight channels. Compared to the straight duct, the highest performance factor, PF = 4.46 was obtained in the rectangular-circular hybrid channel at Re = 10000. Compared to the rectangular wavy duct, the highest performance factor, PF = 1.22 was obtained in the rectangular-circular hybrid channel at Re = 2000.

v) The results of the present numerical study have revealed that higher heat transfer and performance factor can be achieved if the hybrid wave profile is preferred instead of the uniform wave profile.

In future studies, the effects of hybrid models of corrugated channels with different geometries on flow and heat transfer can be studied for different flow regimes and different fluid types. In addition, flow and heat transfer behaviors can be examined experimentally and numerically by adding different turbulators to hybrid corrugated channels.

ACKNOWLEDGEMENT

The author would like to express gratitude to Çankırı Karatekin University, Turkey for providing research facilities. This research received no specific grant from any funding agency in the public, commercial, or not-for-profit sectors.

CONFLICT OF INTEREST

No potential conflict of interest was reported by the authors.

AUTHORS CONTRIBUTION

D. Uysal: Visualisation; Original draft preparation.

S. Akçay: Conceptualization; Methodology; Formal analysis and investigation; Writing – original draft preparation; Writing – review and editing; Supervision.

REFERENCES

[1] E. A. Handoyo, D. Ichsani, "Numerical studies on the effect of delta-shaped obstacles' spacing on the heat transfer and pressure drop in V-corrugated channel of solar air heater," *Solar Energy*, vol. 131, pp. 47-60, 2016.

[2] H. Ameur, D. Sahel, "Effect of some parameters on the thermo-hydraulic characteristics of a channel heat exchanger with corrugated walls," *Journal of Mechanical and Energy Engineering*, vol. 3, pp. 53-60, 2019.

[3] A. Kaood, M. A. Hassan, "Thermo-hydraulic performance of nanofluids flow in various internally corrugated tubes," *Chemical Engineering and Processing-Process Intensification*, vol. 154, p. 108043 2020.

[4] R. K. Ajeel, W. I. Salim, K. Hasnan, "Experimental and numerical investigations of convection heat transfer in corrugated channels using alumina nanofluid under a turbulent flow regime," *Chemical Engineering Research and Design*, vol. 148, pp. 202–217, 2019.

[5] L. Matysiak and R. Platek, "Analytical, numerical, and experimental study of a robot controller with a forced cooling system," *Heat Transfer Research*, vol. 50, no. 2, pp. 195-216, 2019.

[6] M. Khan, S. Z. Shuja, B. S. Yilbas, and H. Al-Qahtani, "A case study on innovative design and assessment of a microchannel heat sink with various turbulators arrangements," *Case Studies in Thermal Engineering*, vol. 31, p. 101816, 2022.

[7] I. Afaynou, H. Faraji, K. Choukairy, A. Arshad, M. Arıcı, "Heat transfer enhancement of phase-change materials (PCMs) based thermal management systems for electronic components: A review of recent advances," *International Communications in Heat and Mass Transfer*, vol. 143, p. 106690, 2023.

[8] J. M. Wua, J. Zhao, "A review of nanofluid heat transfer and critical heat flux enhancement research gap to engineering application," *Progress in Nuclear Energy*, vol. 66, pp. 13-24, 2013.

[9] T. Alam, M. H. Kim, "A comprehensive review on single phase heat transfer enhancement techniques in heat exchanger applications," *Renewable and Sustainable Energy Reviews*, vol. 81, pp. 813-839, 2018.

[10] J. Zhang, X. Zhu, M. E. Mondejar, F. Haglind, "A review of heat transfer enhancement techniques in plate heat exchangers," *Renewable and Sustainable Energy Reviews*, vol. 101, pp. 305-328, 2019.

[11] S. S. M. Ajarostaghi, M. Zaboli, H. Javadi, B. Badenes, J. F. Urchueguia, "A review of recent passive heat transfer enhancement methods," *Energies*, vol. 15, p. 986, 2022.

[12] S. Akcay, "Numerical analysis of heat transfer improvement for pulsating flow in a periodic corrugated channel with discrete V-type winglets," *International Communications in Heat Mass Transfer*, vol. 134, p. 105991, 2022.

[13] Z. Brodniansk´a, S. Kot˘smíd, "Heat transfer enhancement in the novel wavy shaped heat exchanger channel with cylindrical vortex generators," *Applied Thermal Engineering*, vol. 220, p. 119720, 2023.

[14] S. Akcay, U. Akdag, "Heat transfer enhancement in a channel with inclined baffles under pulsating flow: A CFD study," *Journal of Enhanced Heat Transfer*, vol. 30, no. 5, pp. 61-79, 2023.

[15] W. He, D. Toghraie, A. Lotfipour, F. Pourfattah, A. Karimipour, M. Afrand, "Effect of twisted-tape inserts and nanofluid on flow field and heat transfer characteristics in a tube," *International Communications in Heat and Mass Transfer*, vol. 110, p. 104440, 2020.

[16] R. H. Monfared, M. Niknejadi, D. Toghraie, P. Barnoon, "Numerical investigation of swirling flow and heat transfer of a nanofluid in a tube with helical ribs using a two-phase model," *Journal of Thermal Analysis and Calorimetry*, vol. 147, no. 4, pp. 3403–3416, 2022.

[17] C-N. Feng, C-H. Liang, Z-X. Li, "Friction factor and heat transfer evaluation of cross-corrugated triangular flow channels with trapezoidal baffles," *Energy & Buildings*, vol. 257, p. 111816, 2022.

[18] L. K. Nitturi, V. K. S. Kapu, R. Gugulothu, A. Kaleru, V. Vuyyuri, A. Farid, "Augmentation of heat transfer through passive techniques," *Heat Transfer*, vol. 52, no. 6, pp. 4422-4449, 2023.

[19] N. Kurtulmus, B. Sahin, "A review of hydrodynamics and heat transfer through corrugated channels," *International Communications in Heat and Mass Transfer*, vol. 108, p. 104307, 2019.

[20] D. Haridas, V. Singh, A. Srivastava, "An experimental investigation of heat transfer performance of wavy channels under laminar flow conditions: An interferometric study," *Journal of Enhanced Heat Transfer*, vol. 27, no. 6, pp. 561-576, 2020.

[21] K. Kumar, R. Kumar, R. S. Bharj, P. K. Mondal, "Irreversibility analysis of the convective flow through corrugated channels: A comprehensive review," *The European Physical Journal Plus*, vol. 136, no. 4, pp. 1–40, 2021.

[22] M. A. Alfellag, H. E. Ahmed, M. G. Jehad, A. A. Farhan, "The hydrothermal performance enhancement techniques of corrugated channels: A review," *Journal of Thermal Analysis and Calorimetry*, vol. 147, pp. 10177-10206, 2022.

[23] M. Esmaeili, K. Sadeghy, M. Moghaddami, "Heat transfer enhancement of wavy channels using Al_2O_3 nanoparticles," *Journal of Enhanced Heat Transfer*, vol. 17, no. 2, pp. 139-151, 2010.

[24] P. M. Mithun Krishna, M. Deepu, S. R. Shine, "Numerical investigation of wavy microchannels with rectangular cross section," *Journal of Enhanced Heat Transfer*, vol. 25, no. 4-5, pp. 293-313, 2018.

[25] B. Saleh, L.S. Sundar, "Experimental study on heat transfer, friction factor, entropy and exergy efficiency analyses of a corrugated plate heat exchanger using Ni/water nanofluids," *International Journal of Thermal Sciences*, vol. 165, p. 106935, 2021.

[26] W. Wang, Y. Zhang, J. Liu, B. Li, B. Sund´en, "Numerical investigation of entropy generation of turbulent flow in a novel outward corrugated tube," *Journal of Heat and Mass Transfer*, vol. 126, pp. 836–847, 2018.

[27] R. K. Ajeel, W. Saiful-Islam, K. Sopian, M. Z. Yusoff, "Analysis of thermal-hydraulic performance and flow structures of nanofluids across various corrugated channels: An experimental and numerical study," *Thermal Science and Engineering Progress*, vol. 19, p. 10060, 2020.

[28] F. Ahmad, S. Mahmud, M. M. Ehsan, M. Salehin, "Numerical assessment of nanofluids in corrugated minichannels: Flow phenomenon and advanced thermo-hydrodynamic analysis," *International Journal of Thermofluids*, vol. 20, p. 100449, 2023.

[29] M. Khoshvaght-Aliabadi, "Influence of different design parameters and Al_2O_3-water nanofluid flow on heat transfer and flow characteristics of sinusoidal-corrugated channels," *Energy Conversion and Management*, vol. 88, pp. 96–105, 2014.

[30] M. E. Nakhchi, "Experimental optimization of geometrical parameters on heat transfer and pressure drop inside sinusoidal wavy channels," *Thermal Science and Engineering Progress*, vol. 9, pp. 121–131, 2019.

[31] R. K. Ajeel, W. I. Salim, K. Hasnan, "Design characteristics of symmetrical semicircle- corrugated channel on heat transfer enhancement with nanofluid," *International Journal of Mechanical Sciences*, vol. 151, pp. 236–250, 2019.

[32] H. Togun, R. Z. Homod, Z. M. Yaseen, A. M. Abed, J. M. Dhabab, R. K. Ibrahem, et al., "Efficient heat transfer augmentation in channels with semicircle ribs and hybrid Al_2O_3-Cu/water nanofluids," *Nanomaterials*, vol. 12, no. 15, p. 2720, 2022.

[33] S. Akcay, "Heat transfer analysis of pulsating nanofluid flow in a semicircular wavy channel with baffles," *Sādhanā*, vol. 48, no. 57, 2023.

[34] L. Z. Zhang, "Numerical study of periodically fully developed flow and heat transfer in cross-corrugated triangular channels in transitional flow regime," *Numerical Heat Transfer, Part A: Applications*, vol. 48, no. 4, pp. 387–405, 2005.

[35] S. K. Mehta, S. Pati, "Analysis of thermo-hydraulic performance and entropy generation characteristics for laminar flow through triangular corrugated channel," *Journal of Thermal Analysis Calorimetry*, vol. 136, 1, pp. 49–62, 2019.

[36] E. N. Krishnan, H. Ramin, A. Guruabalan, C. J. Simonson, "Experimental investigation on thermo-hydraulic performance of triangular cross-corrugated flow passages," *International Communications in Heat and Mass Transfer*, vol. 122, p. 105160, 2021.

[37] Z-X. Li, S-Q. Sung, C. Wang, C-H. Liang, S. Zeng, T. Zhong, et al., "The effect of trapezoidal baffles on heat and flow characteristics of a cross-corrugated triangular duct," *Case Studies in Thermal Engineering*, vol. 33, p. 101903, 2022.

[38] A. M. Abed, M. A. Alghoul, K. Sopian, H. A. Mohammed, A. N. Al-Shamani, "Design characteristics of corrugated trapezoidal plate heat exchangers using nanofluids," *Chemical Engineering Processing: Process Intensification*, vol. 87 pp. 88–103, 2015.

[39] R. K. Ajeel, W. I. Salim, K. Hasnan, "Influences of geometrical parameters on the heat transfer characteristics through symmetry trapezoidal-corrugated channel using SiO_2-water nanofluid," *International Communications Heat Mass Transfer*, vol. 101, pp. 1–9, 2019.

[40] H. Zontul, H. Hamzah, N. Kurtulmuş, B. Şahin, "Investigation of convective heat transfer and flow hydrodynamics in rectangular grooved channels," *International Communications in Heat and Mass Transfer*, vol. 126, p. 105366, 2021.

[41] R. K. Ajeel, R. Zulkifli, K. Sopian, S. N. Fayyadh, A. Fazlizan, A. Ibrahim, "Numerical investigation of binary hybrid nanofluid in new configurations for curved- corrugated channel by thermal-hydraulic performance method," *Powder Technology*, vol. 385, pp. 144–159, 2021.

[42] Y. Zheng, H. Yang, H. Mazaheri, A. Aghaei, N. Mokhtari, M. Afrand, "An investigation on the influence of the shape of the vortex generator on fluid flow and turbulent heat transfer of hybrid nanofluid in a channel," *Journal of Thermal Analysis and Calorimetry*, vol. 143, pp. 1425–1438, 2021.

[43] M. Khan, I. N. Alsaduni, M. Alluhaidan, W-F. Xia, M. Ibrahim, "Evaluating the energy efficiency of a parabolic trough solar collector filled with a hybrid nanofluid by utilizing double fluid system and a novel corrugated absorber tube," *Journal of the Taiwan Institute of Chemical Engineers*, vol. 124, pp. 150-161, 2021.

[44] H. A. Mohammed, A. M. Abed, M. A. Wahid, "The effects of geometrical parameters of a corrugated channel with in out-of-phase arrangement," *International Communications in Heat and Mass Transfer*, vol. 40, pp. 47-57, 2013.

[45] M. K. Aktas, O. Baser, S. R. Angeneh, "Effects of pulsating flow on convection in wavy channels with phase shift," *Heat Transfer Research*, vol. 51, no. 9, pp. 865-878, 2020.

[46] R. K. Ajeel, W. S-I. W. Salim, K. Hasnan, "Thermal and hydraulic characteristics of turbulent nanofluids flow in trapezoidal-corrugated channel: Symmetry and zigzag shaped," *Case Studies in Thermal Engineering*, vol. 12, pp. 620–635, 2018.

[47] R. K. Ajeel, W. I. Salim, K. Sopian, M. Z. Yusoff, K. Hasnan, A. Ibrahim, et al., "Turbulent convective heat transfer of silica oxide nanofluid through corrugated channels: an experimental and numerical study," *International Journal of Heat Mass Transfer*, vol. 145, p. 118806, 2019.

[48] T. Choudhary, M. K. Sahu, V. Shende, A. Kumar, "Computational analysis of a heat transfer characteristic of a wavy and corrugated channel," *Material Today: Proceedings*, vol. 56, pp. 263-273, 2022.

[49] A. Naderifar, M. Nikian, K. Javaherdeh, M. Borji, "Numerical investigation of the effect of fins on heat transfer enhancement of a laminar non-newtonian nanofluid flow through a corrugated channel," *Journal of Thermal Analysis and Calorimetry*, vol. 147, pp. 9779-9791, 2022.

[50] L. Zhang, D. Che, "Influence of corrugation profile on the thermal hydraulic performance of cross-corrugated plates," *Numerical Heat Transfer, Part A: Applications*, vol. 59, no. 4, pp. 267–296, 2011.

[51] M. Ahmed, M. Yusoff, K. Ng, N. Shuaib, "Effect of corrugation profile on the thermal–hydraulic performance of corrugated channels using CuO–water nanofluid," *Case Studies in Thermal Engineering*, vol. 4, pp. 65-75, 2014.

[52] M. Salami, M. Khoshvaght-Aliabadi, A. Feizabadi, "Investigation of corrugated channel performance with different wave shapes," *Journal of Thermal Analysis and Calorimetry*, vol. 138, no. 5, pp. 3159–3174, 2019.

[53] R. K. Ajeel, W. S-I. W. Salim, K. Hasnan, "Thermal performance comparison of various corrugated channels using nanofluid: Numerical study," *Alexandria Engineering Journal*, vol. 58, pp. 75–87, 2019b.

[54] S. S. Shahsavar, I. B. Alimohammadi, Askari, H. M. Ali, "Numerical investigation of the effect of corrugation profile on the hydrothermal characteristics and entropy generation behavior of laminar forced convection of non-Newtonian water/CMC-CuO nanofluid flow inside a wavy channel," *International Communication in Heat and Mass Transfer*, vol. 121, p. 105117, 2021.

[55] R. K. Ajeel, K. Sopian, R. Zulkifli, "A novel curved-corrugated channel model: thermal-hydraulic performance and design parameters with nanofluid," *International Communications in Heat Mass Transfer*, vol. 120, p. 105037, 2021.

[56] K. Kumar, R. Kumar, R. S. Bharl, "Thermohydraulic performance enhancement using novel hybrid corrugation configuration channels in thermal systems," *International Communications in Heat and Mass Transfer*, vol. 134, p. 105999, 2022.

[57] ANSYS Inc., ANSYS Fluent User Guide & Theory Guide- Release 15.0, USA, 2015.

[58] S. Akcay, "Numerical study of turbulent heat transfer process in different wavy channels with solid and perforated baffles," *Heat Transfer Research*, vol 54, no. 18, pp. 53-82, 2023.

[59] Y. A. Cengel, J. M. Cimbala. Fluid Mechanics, 3rd Ed. New York: Tata McGraw-Hill Education, 2010.

NOMENCLATURE

Abbreviations

CFD	Computational Fluid Dynamics
FVM	Finite Volume Method
PF	Performance Factor
TE	Thermal Enhancement

Symbols

C_p	specific heat (kJ/kgK)
D_h	hydraulic diameter (m)
f	friction factor

Symbols

H	channel height (m)
h	heat transfer coefficient (W/m^{2}K)
L	length of channel (m)
Nu	Nusselt number
q''	heat flux (W/m^2)
Re	Reynolds number
T	temperature (K)
u	average velocity (m/s)
ΔP	pressure drop (Pa)
ΔT_{ln}	logarithmic temperature difference (K)
λ	heat conduction coefficient (W/mK)
μ	dynamic viscosity (Pa.s)
ρ	density of fluid (kg/m^3)
υ	kinematic viscosity (m^2/s)

Subscripts

h	hybrid
in	inlet
o	outlet
rec	rectangular
s	straight
w	wavy, wall